

Orbit Determination for the MICROSCOPE Mission Specificities and Performance

By David PASCAL,¹⁾ John MOYARD,¹⁾ Flavien MERCIER,¹⁾ Pierre-Yves GUIDOTTI,¹⁾ Thomas JUNIQUE,¹⁾ Romain MATHIEU,¹⁾

¹⁾CNES, Toulouse, France

(Received June 21st, 2017)

MICROSCOPE is a drag-free satellite launched in April 2016 into a 710km sun-synchronous orbit, in order to perform a space test of the Weak Equivalence Principle with an accuracy never reached before. This paper presents the role and activities of the CNES orbit determination team in the MICROSCOPE mission. It ranges from the expertise activities in the commissioning phase to the computation of the precise orbit needed for scientific data processing, by going through the specific dynamical context of the drag-free and satellite spin. MICROSCOPE is not only a fundamental physics mission, but also has technical objectives. The in-flight performance analysis of the new spatial GPS single-frequency receiver G-SPHERE-S is one of them, and is presented in this paper on the occasion of its first flight. Thanks to this receiver, the GPS based orbit determination achieves a radial 10cm-accuracy using a L1 ionosphere-free combination, well below the mission requirements. This also provides an opportunity to analyse finely the one-way Doppler measurements which are used as a back-up for orbit determination. The stability of the S-band transceiver downlink frequency is thus examined too, and we show that a metric orbit determination performance can be reached with this one-way Doppler data.

Key Words: orbit determination, MICROSCOPE, drag-free, G-SPHERE-S, one-way Doppler

Nomenclature

CGPS	Cold Gas Propulsion System
CECT	CNES Drag Free expertise group
CNES	French Space Agency
DFACS	Drag Free and Attitude Control System
(W)EP	(Weak) Equivalence Principle
F _{EP}	Equivalence Principle observation Frequency
F _{ORB}	Satellite Orbital Frequency
F _{SPIN}	Satellite Spin Frequency
G-SPHERE-S	SYRLINKS new spatial GNSS receiver
LOF	Local Orbital Frame
OCXO	Oven Controlled X-tal Oscillator
(P)OD	(Precise) Orbit Determination
PSD	Power Spectral Density
RTN	Radial – Tangential – Normal/Cross-track LOF
SUEP/SUREF	EP / Reference Sensor Unit
TM	Test-Mass (T-SAGE includes 4 TM, working by pair)
TSAGE	Twin Space Accelerometer for Gravity Experiment
PVT	Position Velocity Time receiver data
ZOOM	CNES Precise Orbit Determination reference software
ZOOMIC	OD software for MICROSCOPE, based on ZOOM

1. Introduction

MICROSCOPE (for MICRO-Satellite with drag-free Control for the Observation of the Equivalence Principle) is a 300kg drag-free satellite launched on April 25th 2016 into a 710km sun-synchronous orbit for a two-year mission. The associated CNES mission in collaboration with ESA-ONERA-CNRS-OCA-DLR-ZARM, aims to test one of the Einstein's General Relativity fundamental bases, the WEP, down to the 10^{-15} level.¹⁾

Once in mission mode, within the CECT drag-free expertise group, the OD team provides the ground-computed precise orbit which is needed to process the scientific data and extract

the WEP violation signal. The satellite precise positioning is achieved thanks to a new spatial GNSS receiver, G-SPHERE-S, performing its first flight on MICROSCOPE. The analysis of the receiver in-flight performance and raw measurements is one of the technical objectives of the mission. It will be presented in this paper. One-way downlink Doppler measurements, that were initially foreseen to be the only tracking data available,²⁾ are now used as a back-up of GNSS data. The availability of a GPS-based precise orbit offers the opportunity to characterise accurately these Doppler measurements and the Doppler-based OD performance. Mean-term and long-term stability of the downlink reference frequency can also be observed and interesting behaviours have been picked up.

After a brief description of the MICROSCOPE mission, its scientific objectives and the experiment principle, a quick look at the satellite orbit and pointing is given with a description of the Drag-Free and Attitude Control System (DFACS) operating mode.

Then the paper focuses on the following points:

- the specific context of the MICROSCOPE OD: needs and organisation are described, along with an explanation of the orbital dynamics modelling in drag-free mode
- OD team expertise activities during the commissioning phase and their contributions to the DFACS calibration
- G-SPHERE-S measurement analysis and assessment of the OD performance based on L1 GPS ionosphere-free pre-processed data
- One-way Doppler measurement and downlink frequency stability analysis, then Doppler-based achievable OD performance is presented.

2. MICROSCOPE Mission Overview

2.1. Scientific Objectives and Experiment Principle

General Relativity and Quantum theory are still not compatible, and some alternative theories looking for the ultimate unification predict a WEP violation below 10^{-13} . The WEP, as a basis of the Einstein's theory, states the universality of free fall: two bodies placed in the same gravitational field are subjected to the same acceleration, independently of their mass and composition. WEP on-ground measurements are however reaching their limits in terms of precision, and one solution to increase the accuracy is to perform in-space measurements.

MICROSCOPE is testing the WEP by comparing the acceleration experienced by two free-falling Test Masses (TM) in the Earth's gravity field. To this aim, it embarks two ultrasensitive electrostatic differential accelerometers which constitute the T-SAGE instrument developed by ONERA (see Fig. 1). Each accelerometer consists of two coaxial cylindrical TMs whose motion is electrostatically constrained. In one (reference – "SU REF") accelerometer, the TMs are made of the same material to demonstrate the experiment's accuracy; they are made of different materials in the second ("SU EP") accelerometer, which is used to test the WEP.

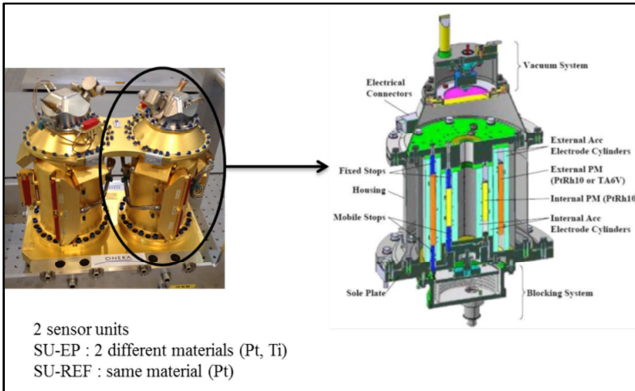


Fig. 1. T-SAGE instrument (on the right SU-REF, on the left SU-EP)

The sensitive axis of the TM is located in the orbital plane, and the satellite is rotating along the cross-track axis. A violation of the EP will produce a relative acceleration of the EP accelerometer at the satellite rotation frequency in the Local Orbital Frame (LOF), the F_{EP} frequency.

2.2. Satellite Orbit and Attitude Guidance

MICROSCOPE flies on a sun-synchronous orbit (ascending node 18h) at 710 km of altitude. The altitude is basically a trade-off between magnitude of the gravitational field, eclipse duration, and propulsion consumption minimisation, that increases when altitude decreases to compensate the drag. MICROSCOPE is a 301 kg microsatellite (1.25m x 0.88m x 1.35m), using a MYRIADE series based platform, with fixed solar panels.

Various pointing modes are available for the different measurement and calibration sessions.³⁾ We will focus here on

the main mission modes: inertial and rotating attitude guidance. Note that at the end of the commissioning phase the inertial pointing mode was abandoned in favour of the spin mode, considered as more appropriate to achieve the mission required accuracy. Figure 2 shows that the EP hypothetical violation signal is modulated at the F_{EP} rotation frequency of the gravity 'g' vector in satellite frame, which is $F_{EP} = F_{ORB} + F_{SPIN}$.

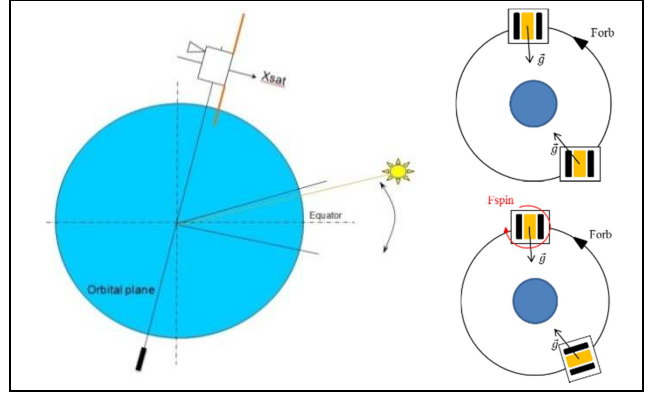


Fig. 2. Microscope orbit (left) and pointing: inertial (top right) and rotating (bottom right). $F_{ORB} \sim 1.68 \cdot 10^{-4}$ Hz

Rotating sessions

The satellite spin axis is the orbit mean cross-track axis, corresponding to X_{SAT} (satellite X axis), and the rotation is forced at the F_{SPIN} frequency. Two values of spin rate, V2 and V3, are now used (the lowest spin rate V1 is no more used):

$$F_{SPIN2} = 9/2 F_{ORB}, \quad w_{EP2} \sim 5.812 \cdot 10^{-3} \text{ rad/s}$$

$$F_{SPIN3} = 35/2 F_{ORB}, \quad w_{EP3} \sim 19.55 \cdot 10^{-3} \text{ rad/s}$$

These science sessions last about 8 days (120 orbits).

Inertial sessions

It is like rotating mode, but with $F_{SPIN} = 0$. Then $F_{EP} = F_{ORB}$, and the EP signal is modulated at the F_{ORB} frequency.

$$w_{ORB} = w_{EP0} \sim 1.0567 \cdot 10^{-3} \text{ rad/s}$$

The pointing is in fact not inertial, since the satellite follows the orbital plane drift, i.e. about $1^\circ/\text{day}$, to ensure the sun-synchronism.

2.3. Drag-free System: Motivation

As said in 2.1, the EP test signal "S" is issued from the difference of acceleration of two T-SAGE TMs:

$$\vec{S} = \vec{\gamma}_1 - \vec{\gamma}_2 = \delta \vec{g} \quad (1)$$

where "g" is the Earth gravitational acceleration and "δ" is the equivalence principle violation parameter.

The Eq. (1) involves a difference between two measurements which have their own errors. More precisely,⁴⁾ but with some simplifications to fit with the scope of this paper and current demonstration, the accelerometer measurements can be written as:

$$\vec{\gamma}_{meas} = \vec{B} + [K] \cdot \vec{\gamma}_{NG} + [Q_2] \cdot \vec{\gamma}_{NG}^2 + \vec{N} \quad (2)$$

where:

$$\overline{\gamma}_{NG} = \overline{g}(G) - \overline{g}(A) + \overline{R}_{In,Cor}(\overline{GA}) + \frac{\overline{F}_{ext}}{M} + \frac{\overline{F}_{thrust}}{M} \quad (3)$$

and:

- B = generalised bias, including the instrumental bias, but also parasitic forces affected by scale factor, coupling and non-linear effects
- K = generalised scale factor including coupling between axis and parasitic forces affected by non-linear effects
- N = instrumental random noise
- Q₂ = quadratic factor (diagonal terms only) taking into account non-linear effects
- γ_{NG} = non-gravitational forces with G and A respectively the centre of mass of the satellite and the TM, $R_{In,Cor}$ the inertial and Coriolis forces and relative acceleration, F_{ext} the external forces (drag, solar pressure, ...), F_{thrust} the propulsion forces

Considering only the scale factor imperfection K_1 and K_2 of two TM, the Eq. (4) shows that the real signal S' also depends, among other effects, on the “common mode” acceleration:

$$\begin{matrix} \gamma_1 \\ \gamma_2 \end{matrix} \quad K_1 \neq K_2 \quad \overline{S}' = (1+K_1)\overline{\gamma}_1 - (1+K_2)\overline{\gamma}_2 = \underbrace{(\overline{\gamma}_1 - \overline{\gamma}_2)}_{diff\ mode} + \underbrace{\left(\frac{K_1+K_2}{2}\right)(\overline{\gamma}_1 - \overline{\gamma}_2)}_{diff\ mode} + \underbrace{(K_1 - K_2)\left(\frac{\overline{\gamma}_1 + \overline{\gamma}_2}{2}\right)}_{common\ mode\ acceleration} \quad (4)$$

The differential scale factor (K_1-K_2) matching accuracy is limited to $1.5 \cdot 10^{-4}$. To achieve the overall mission objective (10^{-15} on δ , i.e. $7.8 \cdot 10^{-15}$ m/s²), the common mode non-gravitational acceleration must remain below 10^{-12} m/s² for low frequency, and in particular around F_{EP} . The non-gravitational forces measured by the TM have thus to be reduced to this level, and that is why the DFACS is needed on MICROSCOPE. The attitude control performance is also subjected to very constraining requirements, with a challenging 10^{-9} rad/s angular rate stability to reach. To meet these stringent requirements, the DFACS relies on the payload accurate accelerations measurements for both linear and angular control. The CGPS, a set of 8 cold gas GAIA-like thrusters, allows the realisation of the commanded thrust that counterbalances the non-gravitational measured forces. The analysis of the in-flight measurements have shown that the DFACS requirements are fully fulfilled.^{5,6)}

3. Orbit Determination Context

3.1. Scientific Needs

A positioning performance of a few meters, needed mainly for an accurate gravity gradient computation⁴⁾, is required for OD accuracy at specific frequencies. These frequencies are connected to the EP signal extraction process. Thus, OD requirements concern positioning biases (DC errors), and positioning errors at F_{EP} , $2 F_{EP}$ and $3 F_{EP}$ frequencies. The errors allocated to OD are given in Table 1.

Table 1. Microscope Orbit Determination performance requirements

Frequency	Radial	Along-track	Cross-track
DC	100 m	100 m	2 m
F_{EP}	7 m	14 m	100 m
2 F_{EP}	100 m	100 m	2 m
3 F_{EP}	2 m	2 m	100 m

However, due to the specificities of orbital dynamics, the satellite is mainly sensitive to constant and F_{ORB} perturbations expressed in the RTN frame. Taking into account this fact, driving errors (in bold characters in Table 1) are cross-track positioning bias and radial-tangential positioning F_{ORB} errors. In rotating modes, the orbit error is not significantly affected by the signals at F_{EP} or F_{SPIN} , as it is showed in 3.3.

3.2. Orbit Determination Activities Within the CECT

OD activities are performed within a specific centre, the CECT. As shown in Fig. 3, the CECT stands between:

- the ground Control Centre (CCC), which checks the satellite’s good health, insures the realisation of the mission plan and provides the telemetry
- the Technological Mission Centre (CMTG), which performs the expertise of G-SPHERE-S receiver
- the scientific Mission Centre (CMS), which monitors the payload (TSAGE), defines the mission plan needs, generates mission data and performs the final evaluation of the EP violation signal.

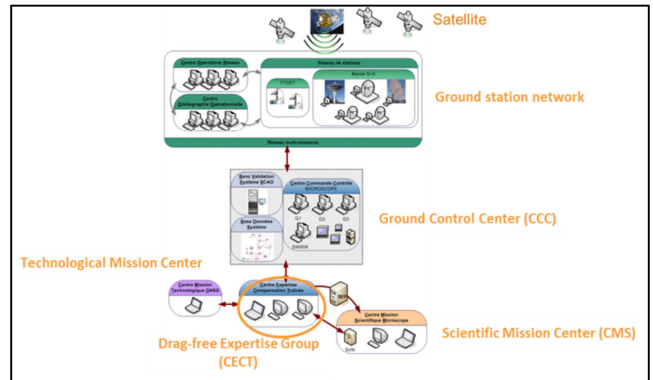


Fig. 3. The CECT as a part of the MICROSCOPE system organisation

The role of CECT is to provide these three entities with all the necessary data. For the OD team, it means:

- preparing the precise orbit provided weekly to CMS
- contributing to the DFACS performance analysis.

Practically, the OD is performed thanks to a specific automated processing chain, named ZOOMIC and based on ZOOM CNES reference POD software. As scientific experimentations are divided into “sessions”, a precise orbit must be computed for each session, within the day following session end. Orbit and associated products (expertise report, error assessment) are then delivered to CMS each week.

3.3. Orbital Dynamics Modelling in Drag-free Mode

The equation of motion applied to the centre of mass A of a

Test Mass (TM), is in an inertial reference frame:

$$\vec{\gamma}(A) = \vec{g}(A) + \vec{\gamma}_{NG} \quad (5)$$

where γ_{NG} is detailed in Eq. 3.

In mission mode, the DFACS is activated and a TM provides acceleration measurements γ_{meas} to the drag-free loop. The control is then applied in A, also named drag-free point. As a result, the DFACS residual acceleration γ_{meas} , given in Eq. (2), is controlled very precisely around zero, and γ_{NG} is the solution of the following Eq. 6 at each time:

$$[K] \cdot \vec{\gamma}_{NG} + [Q_2] \cdot \vec{\gamma}_{NG}^2 = \vec{\gamma}_{meas} + \vec{B} + \vec{N} \quad (6)$$

With a perfect DFACS and no measurement errors, γ_{NG} could be considered as equal to zero, and the satellite should then follow the TM in its free fall around the Earth.

Of course it is not the case, but the analysis of the equation taking into account the magnitude of each term, and focusing on the frequency bandwidth of interest for orbital dynamics [0 – a few F_{ORB}] i.e. [0 – 10^{-3} Hz], shows that we have with a good approximation:

$$\vec{\gamma}_{NG}(t) = \vec{B}_0 \Rightarrow \vec{\gamma}(A) = \vec{g}(A) - \vec{B}_0 \quad (7)$$

where $B_0 = B_0(B, K, Q_2)$ is a constant in the satellite frame, or slowly variable mainly because of B variations.

Elements of Justification

Eq. 6 deserves a dedicated analysis which is not presented here, but the elements leading to the Eq. 7 are given below:

- γ_{meas} : due to the high rejection (about 90 dB for linear accelerations up to the F_{EP} frequency), DFACS residual acceleration⁵⁽⁶⁾ is reduced to less than 10^{-12} m/s² (for harmonic signals around F_{ORB}) and noise PSD $< 2 \cdot 10^{-11}$ m.s²/√f below 10^{-3} Hz, so that noise r.m.s._[0-10⁻³Hz] $< 10^{-12}$ m/s². γ_{meas} can be neglected.
- N: noise PSD $< 10^{-9}$ m.s²/√(10⁻³/f) below 10^{-3} Hz, so noise r.m.s._[0-10⁻³Hz] $< 2 \cdot 10^{-12}$ m/s², N effect can be neglected too
- K (a few 10^{-2} for diagonal, 10^{-3} for transverse terms) and Q_2 ($< 2 \cdot 10^4$ m⁻¹.s²) are constant or slowly variable terms

Content of the B_0 Residual Acceleration

Given the observed magnitude of K and Q_2 , B_0 should be in fact close to B, the instrumental noise. But to minimise gas consumption, B_0 is corrected by the average of the acceleration measurements in open loop. It means that the approximate average - in the satellite frame - of the resulting forces applied to the drag-free point A (external forces, inertial forces due to satellite rotation, and gravity gradient between G and A) are not counterbalanced in drag-free mode. This also explains why B_0 values differ according to the pointing mode.

Moreover, due to various environmental effects, such as thermal variations or parasitic forces, B_0 evolves slightly during measurement sessions. The drift cannot be observed

directly, but it can be deduced from the propulsion command analysis. The maximum drift observed is about 10^{-9} m/s² per day. The perturbing effect on the orbit is very low in rotating mode on all axes (< 1 cm after 8 days).

B_0 Orbit Perturbing Effects

The main perturbing effect of a residual acceleration can be assessed through numerical simulations or analytically with the Hill, Clohessy-Wiltshire equations.¹¹⁾ Illustrative plots are given in Fig. 4 for the following Microscope attitude guidance modes: inertial pointing and V2 spin mode. Representative acceleration values have been taken into account for the simulation, expressed in the satellite frame:

- $B_0v0 = [1.5 \cdot 10^{-7}; 2 \cdot 10^{-8}; 10^{-9}]$ m.s² in inertial pointing mode
- $B_0v2 = [1.5 \cdot 10^{-7}; 10^{-8}; 10^{-8}]$ m.s² in V2 spin mode
- $B_0v3 = [1.5 \cdot 10^{-7}; 1.4 \cdot 10^{-7}; 1.4 \cdot 10^{-7}]$ m.s² in V3 spin mode

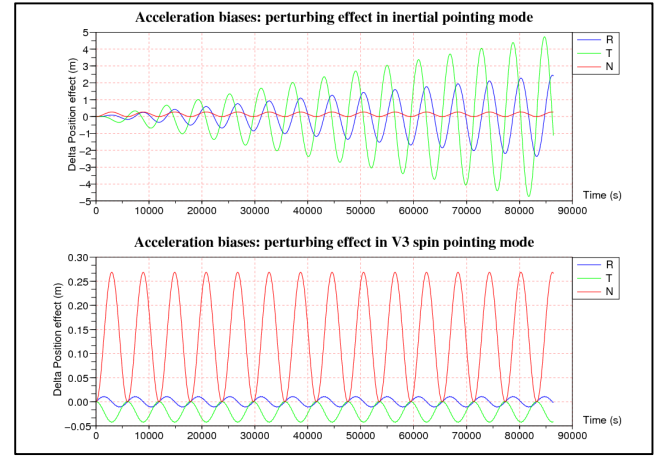


Fig. 4. Example of the perturbing effects of the residual acceleration B_0 , expressed in terms of position difference in the local RTN frame, for inertial pointing and V3 rotating attitude guidance

Hill equations show that orbital dynamics of a quasi-circular orbit is mainly sensitive to constant forces and F_{ORB} forces expressed in the LOF. B_0 in-plane components ($B_{0,Ysat}$, $B_{0,Zsat}$) are seen as F_{EP} perturbing forces in the LOF in which the Hill equations are naturally expressed, whereas $B_{0,Xsat}$ is a constant cross-track acceleration. That is why in-plane residual acceleration B_0 has divergent effect in inertial pointing mode ($F_{EP} = F_{ORB}$): satellite eccentricity grows, making $B_{0,YZ}$ easily observable by OD. It is also the reason why the in-plane residual accelerations do not affect significantly the orbit when the satellite spin rate increases ($F_{EP} \gg F_{ORB}$), with position effect here below 5cm with V3 spin rate. The cross-track effect is a position bias, with the equivalence of 10^{-7} m/s² \Leftrightarrow 9cm (periodic variations are absorbed by the initial state-vector).

Modelling Dynamics for OD purpose

Finally, for orbital dynamics concerns and at our typical OD accuracy level (a few tens cm), the appropriate dynamic modelling in drag-free mission mode is very simple: dynamic

motion is solved at the TM centre of mass used in the control loop (and not the satellite centre of mass), considering only gravitational forces and an effective acceleration bias B_0 . Empirical forces are added to absorb the residual effects described previously (bias and associated low-frequency variations, noise effects), but also to check the quality of the dynamic modelling. In rotating pointing mode, in-plane biases are not observable (effect $<$ a few cm). Cross-track perturbation will be marginally observable in all the pointing modes, because of the limited OD accuracy.

4. Expertise Activities During Commissioning Phase: Accelerometers Data against Modelled Accelerations

The commissioning phase ended in December 2016, after 7 months of a very complex period.⁷⁾ After having faced several difficulties, and some quite major ones, the MICROSCOPE team finally managed to push the whole system to an exceptional level of performance.

During this phase, the OD team was involved in analysis and improvement of tracking measurement (Doppler and GPS), but also in different calibration tests related to the acceleration measurements delivered by T-SAGE. Thanks to the precise orbit computed, it was possible to compare the modelled accelerations to the measured ones to perform various analyses. The results of some of those analyses are briefly presented below.

4.1. Accelerometer Bias Estimation

The acceleration measurements are affected by biases (see Eq.2) that are observable through the OD when the satellite is in an inertial pointing mode, as showed in 3.3. One of the roles devoted to the OD team was the monitoring of these biases: they are expected to evolve slightly with the equipment temperature variation.

The measurement biases are estimated directly as dynamic model parameters when drag-free is activated (see Eq. 7). For example, with a 2-days OD arc-length, bias estimation accuracy is about 10^{-8} m/s² at 3σ for in-plane biases (Y_{sat} and Z_{sat}) and $3 \cdot 10^{-7}$ m/s² at 3σ for the cross-track axis (also equal to X_{sat}). Cross-track bias is not well observed (see 3.3).

The biases can also be estimated by comparison between modelled and measured accelerations when drag-free is off, with a slightly degraded accuracy. As the drag-free is applied to a point (TM centre of mass) located about 10cm from the satellite centre of mass, gravity gradient effects are not negligible (about 10^{-7} m/s²) and must be taken into account in the calculations. The possible propulsion biases are estimated through the OD, and this estimation gives in fact the accuracy of the method. The other natural forces are well mastered or their uncertainties are not significant. It is more the definition of the measurement bias that can be subject to discussion, since it varies slowly with time (see 3.3). For instance, Fig. 5 shows the result of the acceleration comparison for the REF sensor unit on June 6th, 2016, in the sensor local frame. Instrument biases are clearly visible.

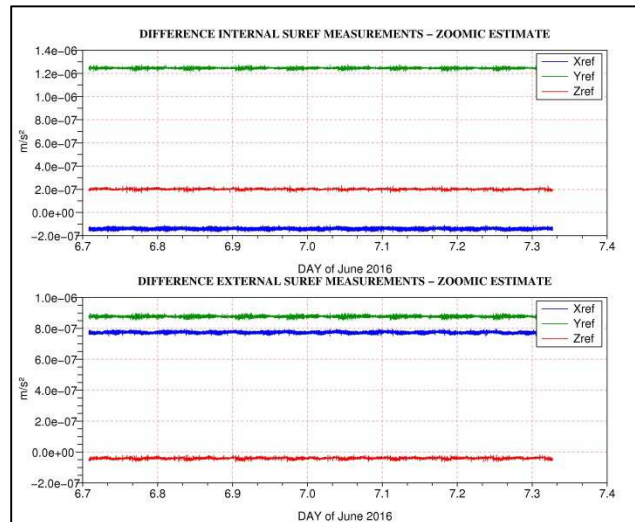


Fig. 5. Difference between measured and estimated accelerations for the REF sensor, over 9 orbits. Residuals are biases at first order.

A good agreement was found between the two possible methods (estimation during drag-free or not) within the precision of the methods. But as the commissioning phase went on, the inertial pointing mode was abandoned in favour of the more competitive spin mode. Bias monitoring was then no more possible through OD, at least for the orbital in-plane components.

4.2. Characterisation of Cold Gas Thrust for Collision Manoeuvre

Although MICROSCOPE is only equipped with cold gas thrusters, limited to a resulting thrust of about $360\mu\text{N}$ ($1.2 \cdot 10^{-6}$ m/s²), it is capable of collision avoidance manoeuvres. The corresponding satellite mode was tested during the commissioning phase: MICROSCOPE was put into a geocentric pointing mode and a constant thrust was performed along the velocity axis (Y-axis) during about 1h. As the pointing was precise - better than 1mrad - and the OD too (about 1m 3D), this test offered the opportunity to analyse at the same time the maximum thrust achievable, to calibrate the thrusters and also the T-SAGE measured accelerations.

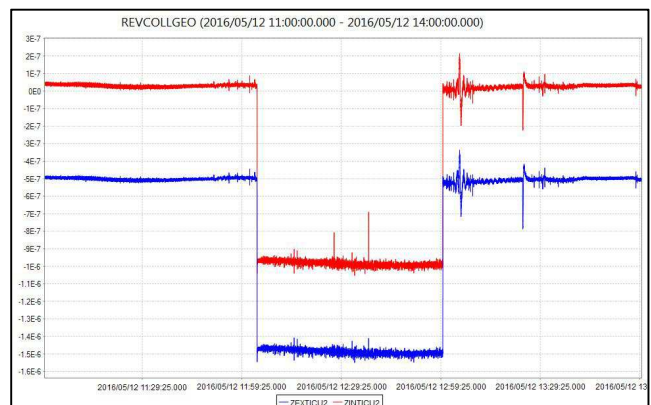


Fig. 6. Accelerations (m/s²) measured by the EP sensor unit during the collision manoeuvre test (REVCOLLGEO)

T-SAGE result. The acceleration step measured by the accelerometers is shown Fig. 6 and demonstrates an underperformance of $14\% \pm 1.5\%$ (SUREF) to about $18\% \pm 2\%$ (SUEP).

Orbit Determination results. A $319.7\mu\text{N}$ thrust with a formal accuracy of $1\mu\text{N}$ is estimated through OD. Another method (energy-based) is also used: the comparison between the semi-major axis for OD before and after the continuous thrust gives a difference of $6.74\text{m} \pm 1\text{cm}$, leading to an along-track thrust of $320.4\mu\text{N}$. Both techniques show an underperformance of 11%.

Discussion. T-SAGE and OD thrust estimations both show an underperformance, but differ from a few percent for the magnitude estimated. The origin of the global underperformance is still under investigation (thrust calibration bias?). The differences between T-SAGE and OD estimations are not completely understood too, whereas differences between SUREF and SUEP measurements can be partly explained by a different scale factor (about 4%).

4.3. Accelerations during Eclipses

During eclipse periods, the Solar Radiation Pressure (SRP) variations measured with T-SAGE can be compared to the modelled ones. This kind of analysis can be used as an indicator of the SRP modelling performance in our OD software ZOOM.

Figure 7 shows a typical example of the modelled accelerations (in black) aligned on measured accelerations (in green), during eclipse. The agreement is good in magnitude and timing, however it can be noticed a difference of behaviour when entering into eclipse and exiting of it: clearly a counter-effect is working here to slow down the SRP effect. A possible explanation could be the thermal response of a satellite whose radiative equilibrium has suddenly changed. The associated infra-red emission magnitude seems consistent with this hypothesis which has to be consolidated yet.

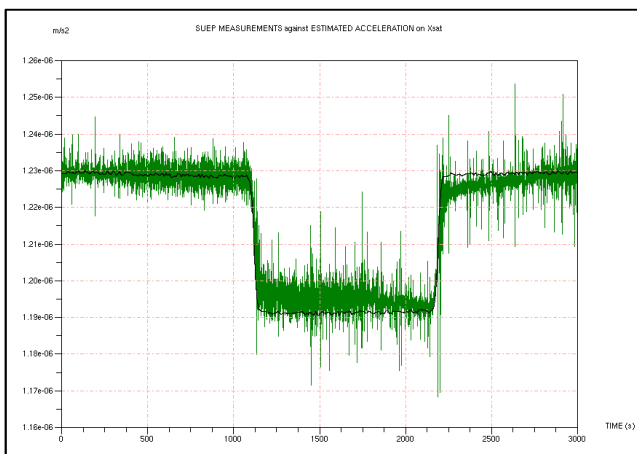


Fig. 7. Example of SUEP measured acceleration (green) against estimated acceleration (black) during eclipse on cross-track axis (Xsat) on the 6th of June, 2016

5. GPS-based Orbit Determination

5.1. G-SPHERE-S Receiver Description and Antennas

G-SPHERE-S is a new spatial single-frequency GPS receiver^{8,9)} manufactured by SYRLINKS, and issued from a CNES R&D program aiming to the design of a low cost GNSS receiver. MICROSCOPE is its first space flight. The mass of the equipment is about 0.9kg for a consumption of less than 4W. The receiver software is highly configurable and performance has already been improved thanks to CNES OD team analysis during ground tests and commissioning phase. Microscope satellite rotates around Xsat, which is also the cross-track axis, and two antennas placed on Xsat opposite faces (see Fig. 8.) are used to collect GPS signals that are transmitted to the receiver via an analogic coupler.

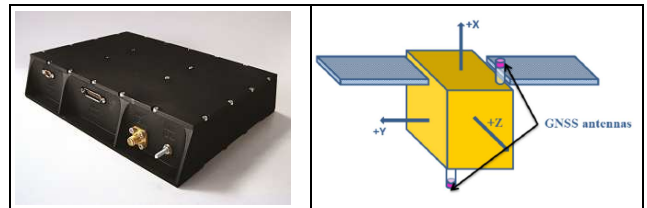


Fig. 8. G-SPHERE-S receiver (Flight Model) and receiver antennas position on Microscope along +/- Xsat (spin and cross-track axis)

5.2. G-SPHERE-S Measurements and Processing

The receiver delivers PVT and L1 C/A code and carrier phase measurements for 9 channels, with a time to first fix below 90s. The default data rate is 10s, but a higher rate (2s) is possible in technical sessions. The receiver clock drift is about 1s/day.

Raw Data Pre-processing

Raw data cannot be used directly in our ZOOM software. Several transformations have to be performed:

- Raw data value interpretation: transmission time is expressed modulo 6s, reception time as seconds from the last reset, etc. => transformation into pseudo range code and phase observables with a usable time tag
- Pseudo-ranges are corrected from Differential Code Bias to build an unbiased code consistent with the GPS clock/ephemeris iono-free solution used (SGU or IGR)
- Code-phase clock correction: currently, code clocks and phase clocks are different ($< 100\text{ns}$). This correction is more cosmetic than needed (no impact on OD).
- Interpolation and reduction: data rate is not constant ($10\text{s} \pm 1\text{s}$), due to a storage request linked to the On Board Computer clock. Data interpolation is needed as ZOOM estimates clocks at a fixed rate, and it has to be done without degrading the data content. The final rate is 60s after this synchronisation (3rd order polynomial fitting), in the nominal mode, and data noise is slightly reduced
- Antenna geometric matching: each GPS measurement is associated with one of the two antennas via a geometric analysis. The number of data in the overlapping regions is naturally low due to low gain antenna.

Note that wind-up effect on the phase measurements has to be taken into account due to the number of satellite rotations.

Ionosphere Perturbations

At an altitude of 710km, code and phase observables are affected by ionosphere delays, whose magnitude can reach several tens of meters, as presented Fig. 8 in the code and phase residuals (computed separately with clocks removed).

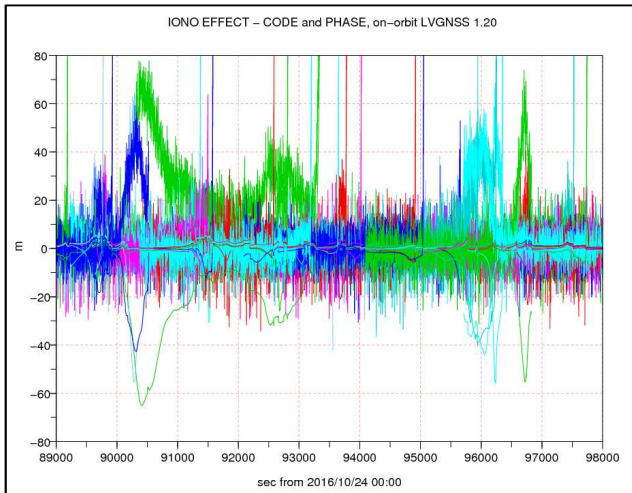


Fig. 8. Example of the opposite perturbing effects of the ionosphere delay for the code (noisy lines) and phase residuals (thin lines)

Similar effects are of course seen in the PVT data, as shown on Fig. 9, the perturbation being particularly high on the radial axis, for a latitude range from -25° to $+50^\circ$. These positions correspond in fact to the sunset, where the high altitude particles are the most excited by the sun, and then the ionosphere effect is the most disturbing. Perturbation effect results in a radial global position bias (9.5m) and higher dispersion (standard deviation 12.5m) than on the other components (no bias and 8m / 4.5m for tangential / cross-track r.m.s. respectively). Note that cross-track GPS Dilution of Precision is two times lower than on radial/tangential axes.

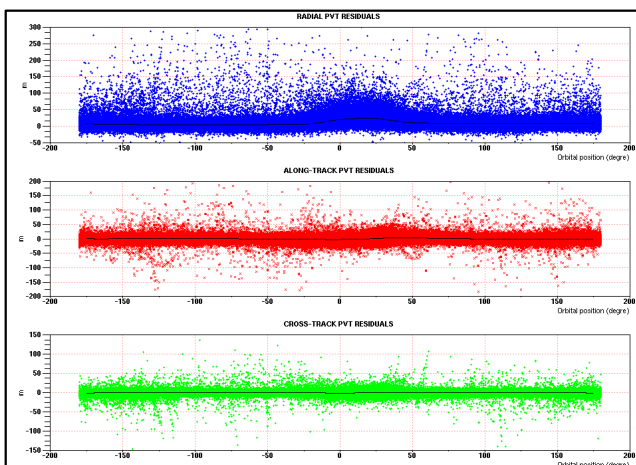


Fig. 9. PVT residuals against satellite orbital position in degree, and expressed in the RTN frame. The black line is the average of residuals.

Ionosphere-free Measurement Characteristics

The major advantage of using an ionosphere-free combination is clear from previous observations: it will allow us not to reject badly ionosphere-affected measurements in the pre-processing, and then to keep the maximum information without being affected by ionosphere very disturbing effects. The combination used is the semi-sum of code and phase data, called GRAPHIC combination. So the resulting noise is the code noise divided by 2, with an ionosphere effect cancelled. We have then better quality measurements, but ambiguities must be identified. An example of ionosphere-free residual after OD is given Fig. 10.

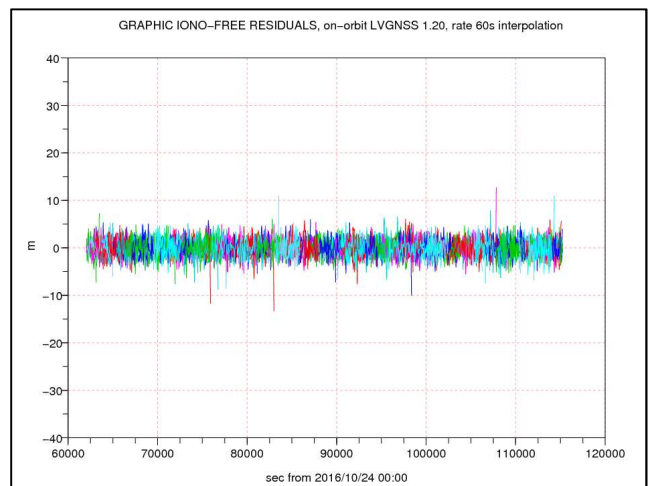


Fig. 10. Ionosphere-free residuals after OD. Data sampling is 60s and result from interpolation

Measurement characteristics are given in Table 2, when not affected too much by ionosphere effect for code and phase.

Table 2. Characteristics of the G-SPHERE-S residuals after OD

Observable	Code	Phase	Ionosphere-free
	no interpolation		interpolation
R.M.S. of the residuals	6m	2mm	2m

5.3. Orbit Determination Performance

The CNES OD team is in charge of providing the POD in mission mode, i.e. in drag-free. GPS ionosphere-free -based, PVT-based and One-Way Doppler-based OD are computed for each scientific session, allowing cross-check analysis. GPS-based OD is the reference orbit.

The performance is controlled through several indicators, such as estimated covariance, orbit overlapping analysis, magnitude of estimated parameters and final OD residuals. The OD accuracy estimate for scientific sessions (120-orbit length) is given in the Table 3, and is well below the OD accuracy requirements (see Table 1).

Table 3. OD accuracy estimate in drag-free mode

component	Radial	Tangential	Cross-track
1σ OD accuracy	10cm	30cm	15cm

Session 120 (V2 spin) is a typical example. Orbit overlapping results are plotted Fig. 11. The consistency with estimated covariance errors is very good. Cross-comparison with PVT-based OD is usually below one meter on the three axes. Estimated empirical forces on tangential axis correspond to the orbit accuracy ($< 10^{-9}$ m/s² for F_{ORB} harmonic and $< 4 \cdot 10^{-12}$ m/s² for constant accelerations). As said in 3.3., the in-plane B_0 residual acceleration is not observable. However, the residual cross-track acceleration $B_{0,Xsat}$ can be observed and estimated at $-2.4 \cdot 10^{-7}$ m/s² (formal accuracy 10^{-7} m/s²), which is consistent with the bias foreseen.

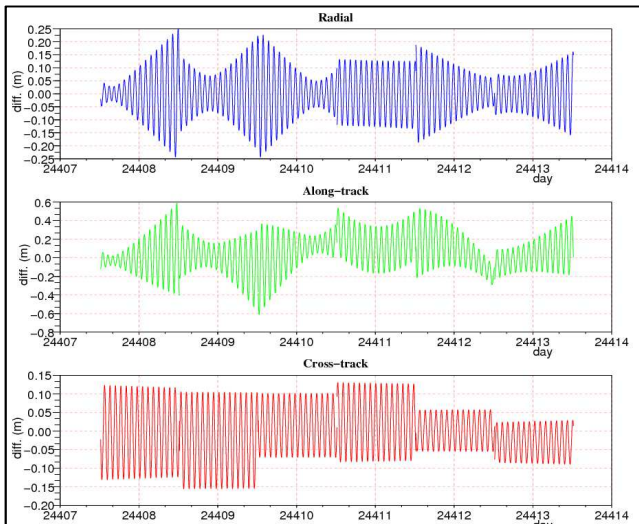


Fig. 11. Position differences in the overlapping regions of sliding OD arcs (2-day arcs, 1-day shift) for session 120, expressed in the RTN frame

6. One-way Doppler-based Orbit Determination

6.1. Motivation and Tracking Characteristics

Motivation and Challenge

Initially foreseen to be the only tracking system available for MICROSCOPE, the one-way Doppler measurements now play a back-up role: in case of a G-SPHERE-S failure, Doppler-based OD shall comply with the position accuracy requirements. Usually used for orbit basic monitoring, reaching a metric position accuracy with these transceiver downlink frequency measurements is a challenge: previous analysis has shown a 10m OD radial precision at best.²⁾

On-board Oscillator

Thus a special care has been taken in the choice of the on-board OCXO equipment, CNES/Syrlinks EWC15 S-band transceivers⁹⁾: indeed the stability of the delivered downlink frequency is a key element of the Doppler measurement performance. Doppler residuals below 0.5 Hz r.m.s. after bias and drift fitting were expected. Two MBDA omnidirectional S-Band antennas placed in opposite direction are simultaneously used for transmission and reception, as shown in Fig. 12. RX1/TX1 and RX2/TX2 transceivers operate alternatively. For OD purpose, the centre of phase of the signal is taken as the mean position of the two antennas.

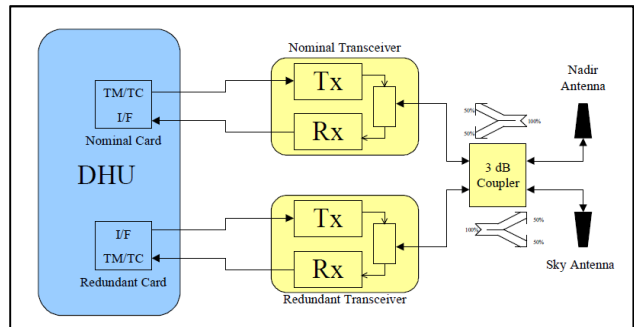


Fig. 12. Microscope Radio-Frequency architecture

Observation Plan

A stable OCXO frequency is not sufficient to achieve the aimed accuracy. The number of collected Doppler data has to be high, at least 7 tracking passes per day, and the geometry of the orbit observation must be various and so well spread among several stations. These requirements are satisfied: seven ground stations from CNES S-Band network compose the observation system, located in Toulouse (Aussaguel and STC) Hartebeesthoek, Inuvik, Kerguelen, Kiruna, and Kourou; an average of 9 tracking passes per day is performed in mission mode.

Measurement Characteristics

A tracking pass lasts about 10min and the measurement are collecting with a 6s rate by the stations. Aboard, one of the two TX is turned ON nominally one minute before the predicted Angle of Sight of 0° (and turned OFF at the end of the pass). RF emission follows in the next minute, increasing the temperature of the RX/TX equipment (about +6°). As TX temperature measures are available during passes, it is possible to estimate the characteristic response time to reach thermal stability: about 6min. It means that 18min are needed to reach 95% of the new equilibrium panel temperature. The stability of TX frequency being linked with these thermal variations, the downlink frequency cannot be stabilised during a tracking pass, and this is what we actually observe in Doppler residuals. An example of the downlink frequency variation is given Fig. 13, in a particular experiment where TX equipment was not turned OFF between HBX and AUS passes, allowing a 30min observation window.

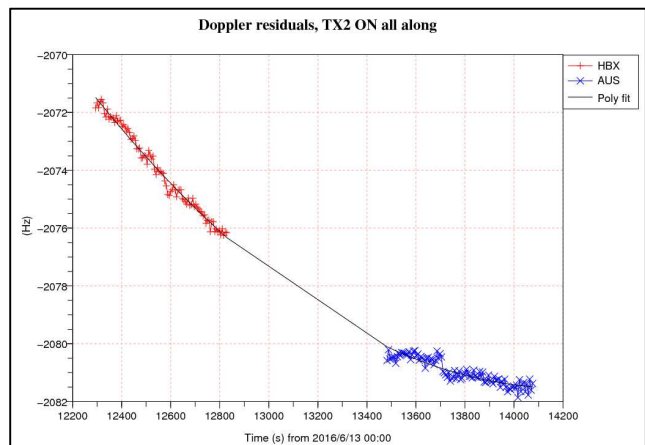


Fig. 13. On-board TX2 reference frequency variations over two Doppler passes (HBX, in red, then AUS, in blue) with TX2 transceiver ON all along. The black curve is a polynomial fitting (2nd order).

Downlink Reference Frequency Evolution Model

The previous considerations show that 0.5Hz one-way Doppler residuals cannot be obtained considering the TX downlink reference frequency as a constant per pass. A drift must also be estimated, and actually a 2nd order polynomial fitting is necessary to be sufficiently representative of the frequency variations during a tracking pass. This is the model used in our OD software (ZOOM). A probably better alternative should be to use an exponential decay model rather than a polynomial one, because it is more representative of the underlying physics; development is ongoing. Applying this exponential model to the frequency variations of Fig. 13 gives a characteristic response time of about 19min. The one-way Doppler residuals after polynomial or exponential fitting present a typical 0.2 Hz r.m.s. level.

6.2. Analysis of the Downlink Frequency Variations

This section aims at analysing the stability of the downlink reference frequency over the passes but also long-term evolution. Abnormal behaviours have been observed and are presented in a second step.

Frequency Stability Analysis

Per pass. The behaviour of a TX emitted frequency is remarkably reproducible from one pass to another, as shown on Fig. 14, and during several days. This is the mark of a similar thermal environment at each pass. However, although reproducible for TX1 or for TX2 considered separately, the behaviour of the two TX is different. Moreover, the characteristics (bias, drift) of this behaviour evolve slowly with the time. Figure 14 also shows that 2nd order polynomial fitting is not always sufficient to absorb the frequency variation, since a residual signal is still visible after the fitting.

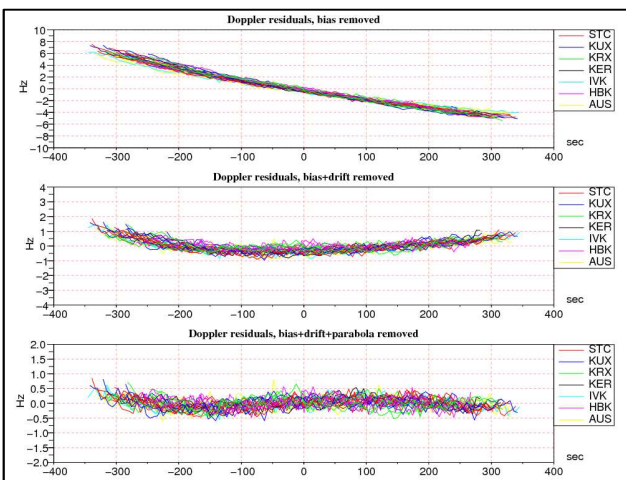


Fig. 14. TX1 transceiver Doppler residuals, time centred at the maximum elevation, for the 3rd to 9th May 2016. Polynomial fitting are done at each of the 29 passes => 3 plots for the 3 different polynomial degrees (0, 1 and 2).

Long term. Frequency long term evolution can be seen through bias or drift variations over long periods. Figure 15 shows the frequency bias for TX2 over almost one month, put in relation with the temperature measured. The correlation is clear. Frequency drift follows a similar pattern.

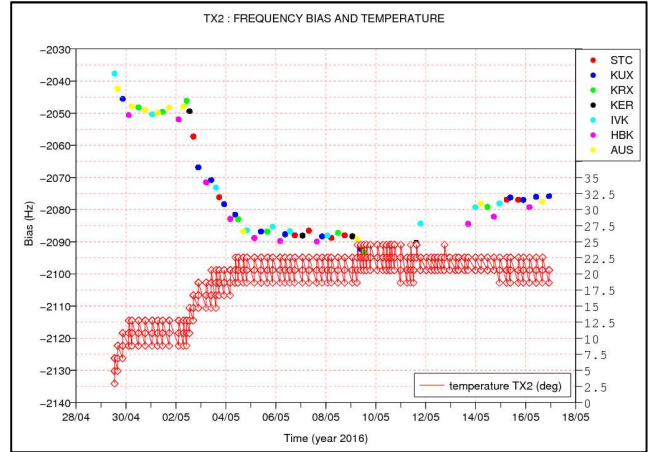


Fig. 15. Downlink frequency long term bias evolution for TX2 transceiver and TX2 associated measured temperature

Frequency Anomalies

Downlink frequency is sometimes affected by sudden jumps (a few Hz from one sample to the next one), but also by frequency stalling (typically a 5Hz increase in 30s), as showed Fig. 16. Jumps can be explained by an activity dip phenomena commonly observed on OCXO. We haven't any explanation yet for frequency stalling that have been seen for about one month on TX2 and then slowly disappeared.

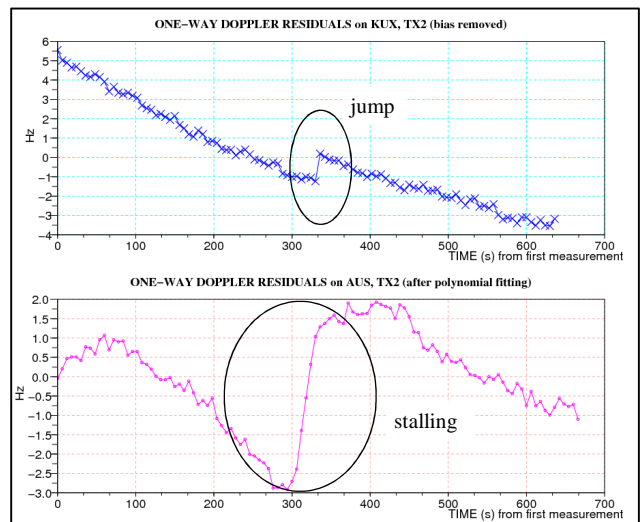


Fig. 16. Example of frequency jumps (on the top) and frequency stalling (on the bottom) in one-way Doppler residuals

6.3. One-way Doppler Orbit Determination Performance

The GPS-based precise orbit offers the opportunity to assess directly the One-Way Doppler OD accuracy, to calibrate the measurements error model, and finally to check

the compliance of Doppler-based OD with the requirements.

Analyses have shown that for an OD arc length of 13 orbits or more in drag-free mode, with a least 5 tracking passes, radial accuracy is below $7m@F_{ORB}$, the most stringent requirement. Actually, submetric or metric radial accuracy are regularly observed in the scientific sessions (120-orbit length), as for session 86 for which the performance is showed Fig. 17. The one-way Doppler measurements are corrected from troposphere and ionosphere perturbations, and 2nd order polynomial fitting of the downlink reference frequency is estimated at each pass. The same dynamic model as GPS-based OD is used (see 3.3).

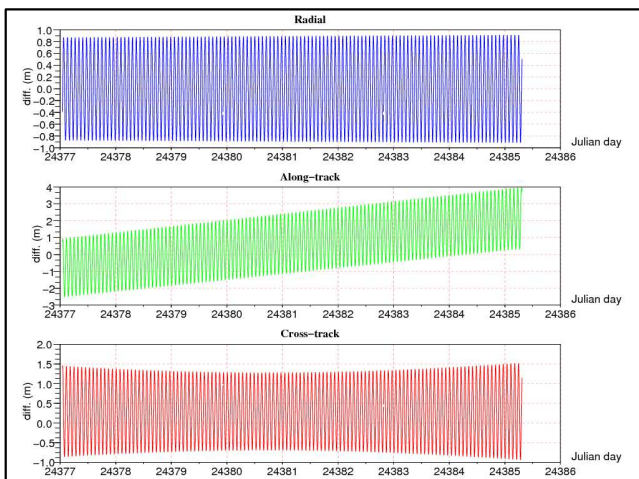


Fig. 17. Position differences between one-way Doppler OD and to GPS reference orbit for session 86 in the RTN frame

Doppler measurements are now fully qualified with respect to the mission requirements. However, the performance has to be monitored, since it is completely driven by the stability of the on-board frequency. And as showed in 6.2, abnormal behaviours sometimes occurred, affecting directly the OD accuracy. For instance, during session 160, frequency stalling described Fig.16 has pushed the radial accuracy around 6m, 3 times higher than the usual performance observed.

7. Conclusion

Thanks to the G-SPHERE-S GPS receiver data, OD performances for MICROSCOPE are not only well better than the required level, but the 10cm-accuracy achieved has also allowed precise analyses of the T-SAGE instrument accelerations and one-way Doppler tracking data. The good performance of the Doppler-based OD, around a few meters, has been demonstrated too, and was not a forgone conclusion.

Beyond that, the MICROSCOPE mission gave us the opportunity to contribute to the in-flight qualification and performance improvement of a new spatial receiver. It was also a chance to practice OD in a quite special dynamic environment, the drag-free, and more broadly, has been a great collective adventure.

Acknowledgments

The authors would like to thank the whole MICROSCOPE project team for making this adventure possible. A special thanks to Pascal PRIEUR, Stéphanie DELAVault, Alain ROBERT, our CECT partners.

References

- 1) J. Bergé, P. Touboul, M. Rodrigues: Status of Microscope, a mission to test the Equivalence Principle in space, 10th International LISA Symposium, May 2014, Gainesville, USA
- 2) S. Delavault, F. Mercier: Orbit Determination for Microscope Satellite Scientific Purpose, AIAA/AAS Astrodynamics Specialist Conference, 21-24 August 2006, Keystone, Colorado, USA
- 3) Cipolla V. et al: Microscope, a Scientific Satellite Development, 25th Annual AIAA/USU Conference on Small Satellite, Logan UT , 9th August 2016
- 4) G. Metris, P. Touboul: First Analysis from the Microscope Mission, Rencontres de Moriond, La Thuile, Italy 2017
- 5) P. Prieur et al.: MICROSCOPE Mission: On-orbit assessment of the Drag-free and Attitude Control System, ISSFD 2017
- 6) Stéphanie Delavault, Pascal Prieur, Thomas Liénart, Alain Robert, Pierre-Yves Guidotti 'MICROSCOPE mission: drag-free and attitude control system expertise activities toward the scientific team', ESA GNC 2017 Salzburg
- 7) Guidotti P-Y, André Y., Cipolla V., Prieur P., Robert A., Rodrigues M., Touboul P., Metris G.: MICROSCOPE: 7 months of a very complex commissioning phase toward ultimate performance, COSPAR 2017 (forthcoming)
- 8) T. Junique et al.: G-SPHERE-S GNSS: New GNSS Receiver for Operational Orbit Restitution of MICROSCOPE Satellite, International Technical Meeting, Monterey, California, USA, January 30-February 2, 2017
- 9) C. Dudal et al.: MICROSCOPE, a CNES microsatellite to check Einstein Equivalence Principle, and its RF equipment 67th International Astronautical Congress (IAC), Guadalajara, Mexico, 26-30 September 2016
- 10) Cipolla V., Dubois J-B., Pouilloux B., Prieur P.: Microscope, a microsatellite for Equivalence Principle Measurement in Space, 25th Annual AIAA/USU Conference on Small Satellites, SCC11-I-3
- 11) O.L. Colombo: The dynamics of global positioning system orbits and the determination of precise ephemerides, Journal of Geophysical Research (ISSN 0148-0227), vol. 94, July 10, 1989, p. 9167-9182